RSC Advances

ROYAL SOCIETY OF CHEMISTRY

www.rsc.org/advances

Journal Name

ARTICLE

A series of tunable emission phosphors of Sm^{3+}, Eu^{3+} and Mn^{2+} doped $Ba_3Tb(PO_4)_3$: Luminescence and energy transfer

Received 00th January 20xx,
Accepted 00th January 20xx

DOI: 10.1039/x0xx00000x

www.rsc.org/

Ting Li, Panlai Li*, Zhijun Wang*, Shuchao Xu, Qiongyu Bai, Zhiping Yang

A series of activators Sm^{3+}, Eu^{3+}, Mn^{2+} ions doped $Ba_3Tb(PO_4)_3$ phosphors with tunable emitting color were synthesized via the high temperature solid state method. The X-ray diffraction, luminescence and fluorescent decay curves were used to characterize the phosphor. The obtained powder crystallizes as a cubic unit cell with space group I-43d. Under 377 nm excitation of Tb^{3+}, $Ba_3Tb(PO_4)_3$:Sm^{3+} not only presents $^5D_4$-$^7F_{6\text{-}3}$ of Tb^{3+} emission lines but also $^4G_{5/2}$-$^6H_{5/2\text{-}9/2}$ of Sm^{3+} orange emission lines, $Ba_3Tb(PO_4)_3$:Eu^{3+} contains the emission lines of Tb^{3+} and Eu^{3+} ($^5D_0$-$^7F_{1\text{-}4}$), and $Ba_3Tb(PO_4)_3$:Mn^{2+} exhibits the emission lines of Tb^{3+} and $^4T_1$-$^6A_1$ orange emission band of Mn^{2+}. In addition, the intensities of red or orange-red emission can be enhanced by tuning the Sm^{3+}, Eu^{3+} and Mn^{2+} contents. The intense emission intensities of Sm^{3+}, Eu^{3+} and Mn^{2+} ions are attributed to the efficient energy transfer from Tb^{3+} to Sm^{3+}, Eu^{3+} and Mn^{2+} ions, respectively, which have been justified through the luminescence spectra and fluorescence decay dynamics. The energy transfer mechanism was demonstrated to be the electric dipole-dipole interaction. For $Ba_3Tb(PO_4)_3$:Sm^{3+}, $Ba_3Tb(PO_4)_3$:Eu^{3+} and $Ba_3Tb(PO_4)_3$:Mn^{2+}, the best quantum efficiencies are 41.6%, 70.3% and 49.8%, respectively. The properties of phosphor indicate that they may be the potential application in UV-pumped white light emitting diodes.

1 Introduction

In recent years, the most common commercial white light emitting diodes (white LEDs) fabricated with a blue chip and a yellow phosphor YAG:Ce^{3+} is un-optimized for indoor use for having emission spectrum deficient in the red region with a result of high correlated color temperature (CCT~7750 K) and low color rendering index (CRI~70-80).[1] Therefore, as an alternative, a combination of near-ultraviolet (n-UV) LED or ultraviolet (UV) LED with red, green and blue emitting phosphors has been developed to improve the CRI, color stability and to tune CCT value, however, one of the key factors limiting the progress of the white LEDs is the general lack of red emitting phosphors that can improve the performance of white light blends in the terms of color rendering and lumen equivalency.[2, 3] Generally, the trivalent europium (Eu^{3+}) ion has been recognized as an excellent activator in many red phosphors due to the $^5D_0$-$^7F_{J(J=0, 1, 2, 3, 4)}$ transitions of Eu^{3+}.[4-6] For the Eu^{3+}-doped phosphors, the excitation lines via the characteristic f-f transitions of Eu^{3+} locate at ultraviolet region. However, in the region of 300-380 nm, Eu^{3+}-doped phosphors have a weak absorption, thus, it is necessary to find a sensitizer for Eu^{3+} luminescence.[7-10] In fact, taking account of Sm^{3+} $^4G_{5/2}$-^6H_J emission in the red region, it is interesting to develop Sm^{3+} activated samples since such phosphors are expected to possess superior red color purity.[11-13] Nevertheless, for Sm^{3+}, the low oscillator strength and narrow line width of Sm^{3+} 4f-4f absorption transitions lead to a weak absorption in 300-380 nm UV region.[11-13] Generally, the host-sensitizer sensitization effect has been utilized to sensitize Sm^{3+} emission, where V^{5+}-O^{2-} charge transfer (CT) transitions are involved.[14] However, for CT emission, the Stokes shift is very large, therefore, this sensitization effect is limited by the low efficiency of charge transfer transitions in UV excitation. Moreover, it is known that emission of Mn^{2+} ion varies from green to red, depending on the influence of crystal field.[15] Owing to the forbidden $^4T_1$-$^6A_1$ transition of Mn^{2+} ion, the emission intensity of Mn^{2+} ion singly doped phosphor is low under UV excitation, and its emission intensity can be considerably enhanced by introducing the efficient sensitizer. Eu^{2+} or Ce^{3+} ions with 4f-5d allowed transition, are normally used as sensitizer to enhance the emission intensity of Mn^{2+} due to the high transition efficiency.[16, 17]

Tb^{3+}, a well-known activator, can emit a green color owing to its general $^5D_4$-$^7F_5$ transtion, and can transfer its energy to another ions.[18] However, the Tb^{3+} ions have a weak absorption in n-UV and visible region, which cannot meet the requirement for the phosphor for white LEDs. Therefore, to overcome this drawback, a host lattice with high concentration of Tb^{3+}, without causing serious concentration quenching, is needed. Accoring the above reason, in the present work, we selected the eulytite-type ortho-phosphate, $Ba_3Tb(PO_4)_3$, as the mother structure, and we aim to develop a novel n-UV convertible phosphor based on the efficient Tb^{3+}-activators (Eu^{3+}, Sm^{3+}, Mn^{2+}) energy transfer and have an insight into the related mechanism. Eulytite-type orthophosphates with the general formula $M_3^{I}M^{II}(PO_4)_3$ (M^{I}=Ca, Sr, Ba and Pb; M^{II}=La, Y, Sc, Bi, Tb and In) have attracted extensive attention as host materials for lanthanide activators because of their excellent thermal stability and optical property.[19-25] In the eulytite-type orthophosphate structure, RE^{3+} (RE=La, Tb, Eu) ions are isolated by the surrounding PO_4 groups, a lower concentration quenching effect can be expected from this crystal character, making the corresponding compound, $Ba_3Tb(PO_4)_3$, suitable as the host for the aim of the work.

[a] College of Physics Science & Technology, Hebei Key Lab of Optic-Electronic Information and Materials, Hebei University, Baoding 071002, China
† li_panlai@126.com; wangzj1998@126.com
Electronic Supplementary Information (ESI) available: [details of any supplementary information available should be included here]. See DOI: 10.1039/x0xx00000x

In the present work, a series of Ln^{3+} (Ln=Eu, Sm) and Mn^{2+} doped $Ba_3Tb(PO_4)_3$ were synthesized to evaluate the potential for white LEDs application and analyze the Tb^{3+}-activators energy transfer, and the luminescence and the color hue tuning and quantum efficiency mechanism were analyzed.

2 Experimental

2.1 Sample preparation

$BaCO_3$ (Analytical Reagent, A. R.), $NH_4H_2PO_4$ (A. R.), Tb_4O_7 (99.99%), Sm_2O_3 (99.99%), Eu_2O_3 (99.99%) and $MnCO_3$ (A. R.) were used as the raw materials. A series of $Ba_3Tb(PO_4)_3$, $Ba_3Eu(PO_4)_3$, $Ba_3Sm(PO_4)_3$, $Ba_3Tb_{1-x}(PO_4)_3$:xSm^{3+}, $Ba_3Tb_{1-y}(PO_4)_3$:yEu^{3+}, $Ba_{3-z}Tb(PO_4)_3$:zMn^{2+} (*x*, *y* and *z*, molar concentration) samples were synthesized by the high temperature solid-state method. The stoichiometric amount of raw materials was thoroughly mixed and ground by an agate mortar and pestle for more than 30 min till they are uniformly distributed. For $Ba_3Tb(PO_4)_3$, and Sm^{3+} (Eu^{3+}) doped samples, the obtained mixtures are heated at 1150 • for 4 h in an air, however, for Mn^{2+} doped samples, the obtained mixtures are heated at 1150 ℃ for 4 h in the presence of reducing atmosphere (5%H_2/95%N_2), and then these obtained samples were cooled to room temperature and ground again in an agate mortar.

2.2 Materials characterization

Phase formation of phosphors is carefully checked by powder X-ray diffraction (XRD) analysis (Bruker AXS D8 advanced automatic diffractometer (Bruker Co., German)), with Ni-filtered Cu Kα1 radiation (λ=0.15405 nm) operating at 40 kV and 40 mA, and a scan rate of 0.02°/s is applied to record the patterns in the 2ϑ range from 10° to 70°. The photoluminescence spectra, luminescence decay curves and quantum efficiency are detected by a FLS920 fluorescence spectrometer, the scanning wavelength range from 200 to 700 nm, a spectral resolution of 0.2 nm, and the exciting sources are a 450 W Xe lamp. Photoluminescence absolute quantum efficiency (QE) was measured by an absolute PL quantum yield measurement system (HORIBA, FL-1057). The diffuse reflection spectra were measured with a Hitachi U4100 UV-VIS-NIR Spectroscopy, scanning at 240 nm/min. Commission International de l'Eclairage (CIE) chromaticity coordinates of sample are measured by a PMS-80 spectra analysis system. All measurements are carried out at room temperature.

3 Results and discussion

3.1 Phase formation

For $Ba_3Tb(PO_4)_3$, $Ba_3Tb_{1-x}(PO_4)_3$:xSm^{3+}, $Ba_3Tb_{1-y}(PO_4)_3$:yEu^{3+} and $Ba_{3-z}Tb(PO_4)_3$:zMn^{2+}, the phase formation were identified by XRD patterns, and a similar XRD patterns are observed for each sample. As a representative, Figure 1 shows the XRD patterns of $Ba_3Tb_{1-x}(PO_4)_3$:xSm^{3+} (*x*=0-0.15). All the diffraction peaks match well with that of the cubic $Ba_3Bi(PO_4)_3$ according to the standard reference of JCPDS card no. 33-0137 (ICSD card no.91803), and no traces of impurity phases are observed. For $Ba_3Tb_{1-y}(PO_4)_3$:yEu^{3+} and $Ba_{3-z}Tb(PO_4)_3$:zMn^{2+}, Figure S1 and S2 depict that there are the similar results. The results indicate the little change of this crystal structure when introduced such Sm^{3+}, Eu^{3+} or Mn^{2+} ions into $Ba_3Tb(PO_4)_3$. According to JCPDS card no. 33-0137 (ICSD card no.91803), $Ba_3Tb(PO_4)_3$ should belong to the eulytite-type compounds, which crystallize in the cubic system with space group I-43d, and the unit cell dimensions are a=b=c=10.4484(2) Å, α=90°, Z=4, Volume (V)=1140.6(2) $Å^3$.[26] As shown in the upper of Figure 1, the general feature of $Ba_3Tb(PO_4)_3$ structure should be regarded as a three-dimensional packing of $[PO4]^{3-}$ anionic tetrahedra and Tb/Ba octahedra, arranged in a manner to share common apices. It is interesting that all the $[PO4]^{3-}$ tetrahedral are totally independent while the Tb/Ba octahedra share edges with each other and form a three-dimensional network.[26]

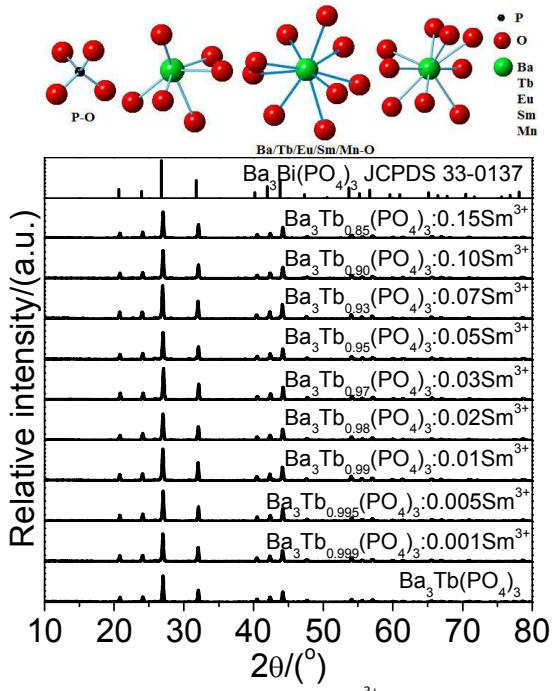

Figure 1. XRD patterns of $Ba_3Tb_{1-x}(PO_4)_3$:xSm^{3+} (*x*=0-0.15). Standard data of $Ba_3Bi(PO_4)_3$ (JCPDS 33-0137) is shown as reference.

3.2 Luminescence properties

As depicted in Figure 2, the reflectance spectra of $Ba_3Tb(PO_4)_3$, $Ba_3Tb(PO_4)_3$:$0.02Sm^{3+}$, $Ba_3Tb(PO_4)_3$:$0.02Eu^{3+}$, $Ba_3Tb(PO_4)_3$:$0.03Mn^{2+}$ phosphors show the similar profiles, which illustrate that the absorptions of phosphors derive from the host. The reflectance spectra present strong energy absorption bands in the region of 200-300 nm. In order to assess the absorption edge from the reflectance spectra, the Kubelka-Munk absorption coefficient (K/S) relationship was availed as follows[27]

$(1-R)^2/2R=K/S$ (1)

where K refers to the absorption coefficient, Represents the reflectivity, and S is the scattering coefficient. From the reflectance spectrum of $Ba_3Tb(PO_4)_3$ host, a roughly evaluated optical band gap is 5.06 eV. Moreover, for the Sm^{3+}, Eu^{3+} or Mn^{2+} doped $Ba_3Tb(PO_4)_3$, the band gap is approximately 5.01 eV.

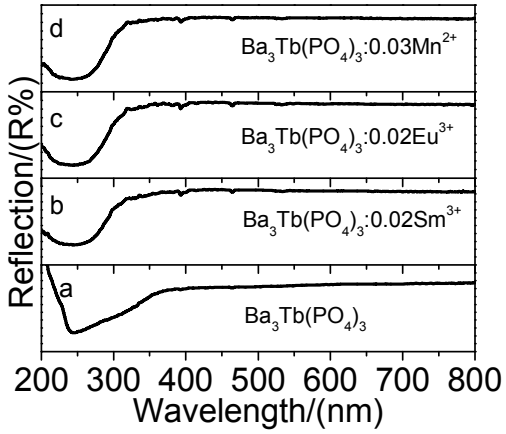

Figure 2. Diffuse reflection spectra of $Ba_3Tb(PO_4)_3$ (a), $Ba_3Tb(PO_4)_3$:$0.02Sm^{3+}$ (b), $Ba_3Tb(PO_4)_3$:$0.02Eu^{3+}$ (c) and $Ba_3Tb(PO_4)_3$:$0.03Mn^{2+}$ (d).

In order to explain the possibility of the Tb^{3+}-Sm^{3+}, Tb^{3+}-Eu^{3+} and Tb^{3+}-Mn^{2+} energy transfer, the luminescent properties of $Ba_3Tb(PO_4)_3$ and $Ba_3Eu(PO_4)_3$ were studied.

Figure 3a described the emission and excitation spectra of $Ba_3Tb(PO_4)_3$. Under 377 nm excitation, the spectrum display a series of emission lines ascribed to the intra-4f^8 $^5D_4$-$^7F_{6-3}$ electronic transitions of Tb^{3+} ions. No emission lines from the $^5D_3$ energy level is observed in the emission spectrum, and the reason can be attributed to high concentration of Tb^{3+} ions, which leads to the occurrence of cross-relaxation. The excitation spectrum of $Ba_3Tb(PO_4)_3$ monitored with the $^5D_4$-$^7F_5$ transition (545 nm) is analyzed in detail. The bands centered at 235 and 250-275 nm are assigned to the spin-allowed (low-spin, LS) and spin-forbidden (high-spin, HS) inter-configurational Tb^{3+} f-d transitions, respectively, and the remaining peaks are assigned to intra-4f^8 transitions between the $^7F_6$ and the $^5F_{5,4}$, $^5H_{7-4}$, $^5D_{1,0}$, $^5L_{10-7}$, $^5G_{6-2}$, and $^5D_{2-4}$ levels.[22] The inset of Figure 3a is a image of $Ba_3Tb(PO_4)_3$ under 365 nm excitation, in which an intense green light can be observed.

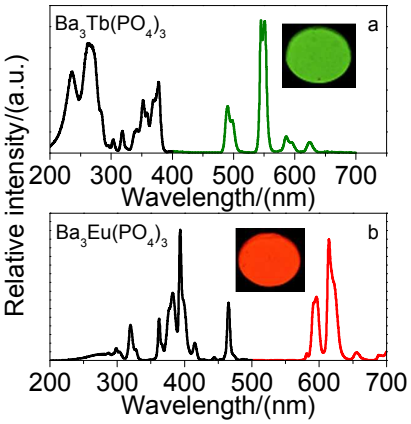

Figure 3. Spectral characteristics of $Ba_3Tb(PO_4)_3$ (a), $Ba_3Eu(PO_4)_3$ (b). Inset: Image of $Ba_3Tb(PO_4)_3$ (a) and $Ba_3Eu(PO_4)_3$ (b) (λ_{ex}=365 nm).

Figure 3b presented the emission and excitation spectra of $Ba_3Eu(PO_4)_3$. Monitored at 615 nm, the excitation spectrum of $Ba_3Eu(PO_4)_3$ displays a weak broad band ranging from 200 to 280 nm, and some narrow peaks (287, 297, 319, 362, 382, 393, 415, 444 and 465 nm, respectively) resulting from the combined absorptions of host and Eu^{3+}-O^{2-} charge transfer (CT) transition, as well as 4f-4f characteristic transitions of Eu^{3+}, respectively. Upon the excitation of f-f transition centered at 393 nm, the emission spectrum presents the characteristic emission lines deriving from the 4f-4f transitions of Eu^{3+} ions in $Ba_3Eu(PO_4)_3$, namely, $^5D_0$ excited states to the ^7F_J ground states including $^5D_0$-$^7F_1$ (596 nm), $^5D_0$-$^7F_2$ (615 nm), $^5D_0$-$^7F_3$ (656 nm) and $^5D_0$-$^7F_4$ (707 nm), respectively.[4-6] And the electric dipole transition $^5D_0$-$^7F_2$ around 615 nm is much stronger than that of the other transitions of Eu^{3+}. Therefore, the inset of Figure 3b depicts $Ba_3Eu(PO_4)_3$ shows an obvious red light.

Generally, Sm^{3+} doped phosphors can exhibit several orange-red emission peaks which are assigned to the $^4G_{5/2}\rightarrow{}^6H_{J/2}$ (J=5, 7 and 9) transitions of Sm^{3+}. However, there is no emission of $Ba_3Sm(PO_4)_3$ in our experiment. The reason should be attributed to high concentration of Sm^{3+} ions, which leads to the occurrence of cross-relaxation.[28]

Actually, Mn^{2+} ions doped eulytite-type orthophosphate can create orange-red emission under UV excitation, for example, our previous results show that $Sr_3La(PO_4)_3$:Mn^{2+} present the orange-red light under 402 nm excitation, and the emission peak locates at 605 nm, therefore, we think that Mn^{2+} doped eulytite-type orthophosphate $Ba_3Tb(PO_4)_3$ should emit orange-red or red light.[23]

In order to explore the energy transfer from Tb^{3+} to Sm^{3+}, Eu^{3+} and Mn^{2+}, a series of samples with the chemical composition of $Ba_3Tb_{1-x}(PO_4)_3$:xSm^{3+}, $Ba_3Tb_{1-y}(PO_4)_3$:yEu^{3+} and $Ba_{3-z}Tb(PO_4)_3$:zMn^{2+} were synthesized and their luminescent properties were investigated.

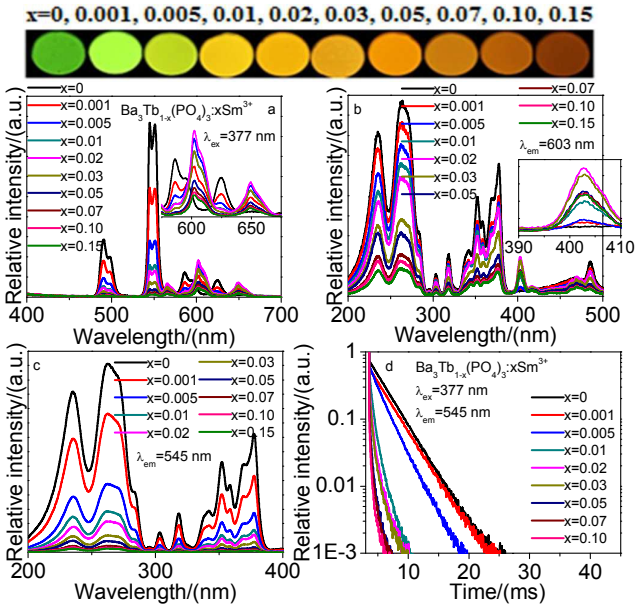

Figure 4. Emission (a, λ_{ex}=377 nm) and excitation (b, λ_{em}=603 nm; c, λ_{em}=545 nm) spectra of $Ba_3Tb_{1-x}(PO_4)_3$:xSm^{3+}, decay curves of $Ba_3Tb_{1-x}(PO_4)_3$:xSm^{3+} (d, λ_{ex}=377 nm, λ_{em}=545 nm).
Inset: Emission spectra of Sm^{3+} (a), excitation spectra of Sm^{3+} (b).
Upper: Image of $Ba_3Tb_{1-x}(PO_4)_3$:xSm^{3+} (λ_{ex}=365 nm).

Figure 4 shows the emission and excitation spectra, and decay curves of $Ba_3Tb_{1-x}(PO_4)_3$:xSm^{3+}. upon excitation of the Tb^{3+} ion f-f transition peak at 377 nm, Figure 4a depicts $Ba_3Tb(PO_4)_3$:Sm^{3+} shows the typical Tb^{3+} and Sm^{3+} ion f-f emission lines. Moreover, with the lower Sm^{3+} concentration, there are both Tb^{3+} and Sm^{3+} emission peaks, and the emission intensities of Tb^{3+} decrease with increasing Sm^{3+} concentration, and the inset of Figure 4a shows the emission intensities of Sm^{3+} have an obvious enhancement. When the Sm^{3+} concentration is higher than x=0.02, not only the Tb^{3+} emission is very weak, but also the emission intensities of Sm^{3+} begin to decrease, the reason is the occurrence of cross-relaxation. And the results can also be seen from the upper image of phosphors. While the excitation spectrum of Sm^{3+} ions consists of typical Tb^{3+} and Sm^{3+} f-f excitation bands, and the excitation intensities, corresponding to Tb^{3+}, directly decrease, however, for the Sm^{3+} excitation intensities (inset of Figure 4b), there are an optimal value at 0.02 Sm^{3+}. For the 545 nm emission of $Ba_3Tb_{1-x}(PO_4)_3$:xSm^{3+}, Figure 4c shows the corresponding excitation spectra, which show the excitation spectrum is similar to that of $Ba_3Tb(PO_4)_3$ sample monitored with the $^5D_4$-$^7F_5$ transition, however, the excitation intensities directly decrease with increasing Sm^{3+} concentration. The above results indicate the Tb^{3+}-Sm^{3+} energy transfer in $Ba_3Tb(PO_4)_3$ are valid.

To further validate the process of energy transfer from Tb^{3+} to activators, under the 377 nm excitation of Tb^{3+}, monitored at 545 nm emission of Tb^{3+}, the decay curves of $Ba_3Tb_{1-x}(PO_4)_3$:xSm^{3+} are measured and shown in Figure 4d. It is known when a donor transfers its energy to an acceptor, the temporal decay of the donor

become fast. Figure 4d shows fluorescence decay curve of Tb^{3+} with different Sm^{3+} concentration. If Tb^{3+} and Sm^{3+} work independently and there is no energy transfer from Tb^{3+} to Sm^{3+}, the luminescence lifetime of both activators will be as same as in single doped samples. If there is energy transfer, the decay of Tb^{3+} excitation state will be accelerated by the energy transfer, and consequently the lifetime of Tb^{3+} will be shortened.

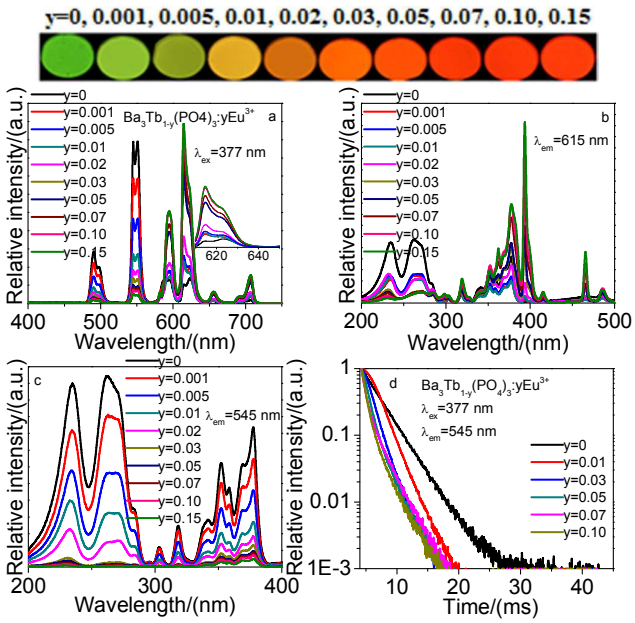

Figure 5. Emission (a, λ_{ex}=377 nm) and excitation (b, λ_{em}=615 nm; c, λ_{em}=545 nm) spectra of $Ba_3Tb_{1-y}(PO_4)_3$:yEu^{3+}, decay curves of $Ba_3Tb_{1-y}(PO_4)_3$:yEu^{3+} (d, λ_{ex}=377 nm, λ_{em}=545 nm).
Inset: Emission spectra of Eu^{3+} (a).
Upper: Image of $Ba_3Tb_{1-y}(PO_4)_3$:yEu^{3+} (λ_{ex}=365 nm).

Figure 5 presents the emission and excitation spectra, and decay curves of $Ba_3Tb_{1-y}(PO_4)_3$:yEu^{3+}. Under 377 nm excitation of Tb^{3+}, it can be observed that the emission spectra are composed of red (615 nm), orange (596 nm) and green (545 nm) light-emitting peaks, which agree well with the results of Ref. [21]. The orange and red emission peaks are attributed to the typical $^5D_0$-^7F_J (J=1, 2) transition emission of Eu^{3+}. The green emission peaks at 545 nm originate from the $^5D_4$-$^7F_5$ transition of Tb^{3+}. With increasing Eu^{3+} concentration, through there are both Tb^{3+} and Sm^{3+} emission peaks in the emission spectra, however, the emission intensities of Tb^{3+} straightly decrease, and that of Eu^{3+} directly increase (as shown in the inset of Figure 5a). *Viz.*, there is no concentration quenching effect in the region of our experiment. And the results can also be seen from the upper image of phosphors. For the 615 nm emission of Eu^{3+}, Figure 5b presents the excitation spectrum of Eu^{3+} ions consists of typical Tb^{3+} and Eu^{3+} f-f excitation bands, in the region of 200-300 nm, which agrees well with the results of Red.[21]. Moreover, there is an obvious decrease of Tb^{3+} excitation intensity with increasing Eu^{3+} concentration. Differently, for the 545 nm emission of $Ba_3Tb_{1-y}(PO_4)_3$:yEu^{3+}, as shown in Figure 5c, the excitation spectrum presents a similar characteristics to that of $Ba_3Tb(PO_4)_3$ sample monitored with the $^5D_4$-$^7F_5$ transition, however, the excitation intensities directly decrease with increasing Eu^{3+} concentration. Therefore, This can prove an energy transfer from Tb^{3+} to Eu^{3+} in $Ba_3Tb(PO_4)_3$:Eu^{3+}. Moreover, Figure 5d shows the decay curves of $Ba_3Tb_{1-y}(PO_4)_3$:yEu^{3+}, and the results show that the lifetimes of Tb^{3+} become shorten with increasing Eu^{3+} concentration. As mentioned above, the results indicate that there should be the energy transfer from Tb^{3+} to Eu^{3+}.

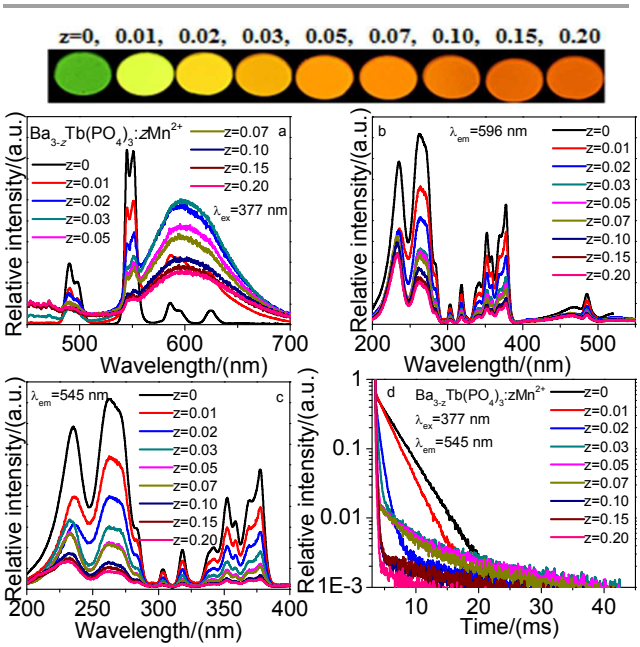

Figure 6. Emission (a, λ_{ex}=377 nm) and excitation (b, λ_{em}=596 nm; c, λ_{em}=545 nm) spectra of $Ba_{3-z}Tb(PO_4)_3$:zMn^{2+}, decay curves of $Ba_{3-z}Tb(PO_4)_3$:zMn^{2+} (d, λ_{ex}=377 nm, λ_{em}=545 nm).
Upper: Image of $Ba_{3-z}Tb(PO_4)_3$:zMn^{2+} (λ_{ex}=365 nm).

Figure 6 presents the emission and excitation spectra, and decay curves of $Ba_{3-z}Tb(PO_4)_3$:zMn^{2+}. Under 377 nm excitation of Tb^{3+}, the emission spectra show the emission characteristics of Tb^{3+} and Mn^{2+}, and the emission intensities of Tb^{3+} decrease with increasing Mn^{2+} doping content, however, that of Mn^{2+} reaches a maximum as *z* equals 0.03 and then begins to decrease due to concentration quenching. And the results can also be seen from the upper image of phosphors. For the Mn^{2+} 596 nm emission, Figure 6b shows the excitation spectrum presents the excitation characteristics of Tb^{3+}, there is no an obvious excitation characteristics of Mn^{2+}. Moreover, for the 545 nm emission of $Ba_{3-z}Tb(PO_4)_3$:zMn^{2+}, as shown in Figure 6c, there are the same excitation peaks between this samples and $Ba_3Tb(PO_4)_3$, however, the excitation intensities directly decrease with increasing Mn^{2+} concentration. Therefore, this may be a direct evidence to demonstrate the energy transfer Tb^{3+}-Mn^{2+} in the $Ba_3Tb(PO_4)_3$ host. As shown in Figure 6d, under the 377 nm excitation of Tb^{3+}, monitored at 545 nm emission of Tb^{3+}, the decay curves of $Ba_{3-z}Tb(PO_4)_3$:zMn^{2+} presents the decrease trend with increasing Mn^{2+} concentration, the results also prove the energy transfer from Tb^{3+} to Mn^{2+}.

Figure 4-6a depicts the emission spectra for $Ba_3Tb_{1-x}(PO_4)_3$:xSm^{3+} (*x*=0-0.15), $Ba_3Tb_{1-y}(PO_4)_3$:yEu^{3+} (*y*=0-0.15) and $Ba_{3-z}Tb(PO_4)_3$:zMn^{2+} (*z*=0-0.20) with different concentration of Sm^{3+}, Eu^{3+} and Mn^{2+}, respectively. We can observe the emission intensities of Tb^{3+} decrease with increasing Sm^{3+}, Eu^{3+} and Mn^{2+} concentrations under 377 nm excitation, and the emission intensities of Sm^{3+} and Mn^{2+} in the $Ba_3Tb(PO_4)_3$ systems clearly increase to the maximum at *x*=0.02 and *z*=0.03, respectively, and subsequently descend with respectively further concentration of Sm^{3+} and Mn^{2+} ions resulting from the concentration effects in Figure 4a and 6a. Differently, the emission intensity of Eu^{3+} keeps an obvious increase with increasing Eu^{3+} concentration in Figure 5a. In order to illuminate the results, these detailed variations of $Ba_3Tb(PO_4)_3$ and activators emission intensities are presented in Figure 7.

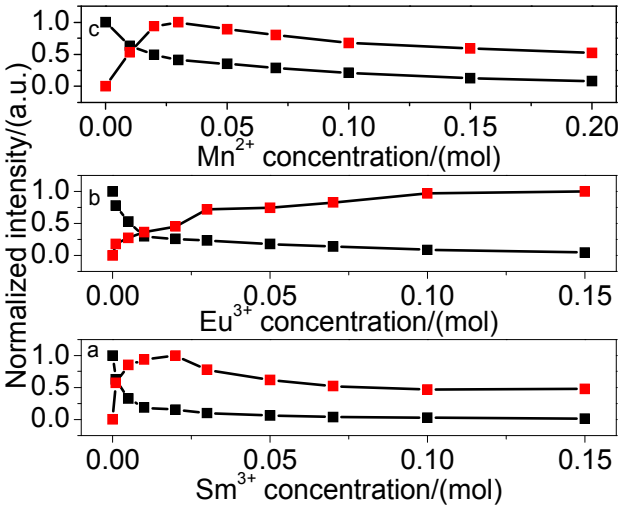

Figure 7. Variation of emission intensity of Tb^{3+} and activators on concentrations in $Ba_3Tb_{1-x}(PO_4)_3$:xSm^{3+} (a), $Ba_3Tb_{1-y}(PO_4)_3$:yEu^{3+} (b) and $Ba_{3-z}Tb(PO_4)_3$:zMn^{2+} (c) (λ_{ex}=377 nm).

The energy transfer efficiencies (η_T) from the Tb^{3+} to activators in $Ba_3Tb_{1-x}(PO_4)_3$:xSm^{3+}, $Ba_3Tb_{1-y}(PO_4)_3$:yEu^{3+} and $Ba_{3-z}Tb(PO_4)_3$:zMn^{2+} systems were calculated using the equation[29-31]

$\eta_T=1-(I/I_0)$ (2)

where η_T refers to the energy transfer efficiency, I_0 and I are luminescent intensities of sensitizer Tb^{3+} in the absence and presence of activator (Sm^{3+}, Eu^{3+} or Mn^{2+}). As shown in Figure 8, the η_T values from Tb^{3+} to activators in $Ba_3Tb_{1-x}(PO_4)_3$:xSm^{3+}, $Ba_3Tb_{1-y}(PO_4)_3$:yEu^{3+} and $Ba_{3-z}Tb(PO_4)_3$:zMn^{2+} systems are plotted as a function of concentrations of Sm^{3+}, Eu^{3+} and Mn^{2+} ions, which show that the η_T values monotonously increase to reach maximums at 98.7%, 95.3% and 91.9% under 377 nm radiation of Tb^{3+}, respectively, indicating the energy transfer from the Tb^{3+} to activators becomes more and more efficient with the increasing concentration of activators ions.

As mentioned above, the shorten lifetime of Tb^{3+} confirms the energy transfer from Tb^{3+} to activators (Sm^{3+}, Eu^{3+} and Mn^{2+}) ions. The decay curves for $Ba_3Tb(PO_4)_3$ can be fitted into a single exponential function as[32]

$I=I_0\exp(-t/\tau)$ (3)

where I_0 and I are the luminescence intensities at time 0 and t, respectively, and t is decay lifetime. On the basis of eqn (3), the lifetime values were determined to be 2.864 ms. However, as illustrated in Figure 4-6d, when incorporated of activators (Sm^{3+}, Eu^{3+} and Mn^{2+}) ions, double-exponential decay behaviour of the activator is observed when the excitation energy is transferred from the Tb^{3+} to activator. Therefore, all of them can be well fitted using a second-order exponential function, and their corresponding decay times can be calculated by the following equation[33-35]

$I=A_1\exp(-t/\tau_1)+A_2\exp(-t/\tau_2)$ (4)

where I is luminescence intensity; A_1 and A_2 are constants; t is time, and τ_1 and τ_2 are lifetimes for rapid and slow decays, respectively. Average lifetimes (τ^*) can be obtained by the formula as follows[33-35]

$\tau^*=(A_1\tau_1^2+A_2\tau_2^2)/(A_1\tau_1+A_2\tau_2)$ (5)

For $Ba_3Tb_{1-x}(PO_4)_3$:xSm^{3+}, $Ba_3Tb_{1-y}(PO_4)_3$:yEu^{3+} and $Ba_{3-z}Tb(PO_4)_3$:zMn^{2+}, the calculated average lifetimes (τ^*) are listed in Table S1. The results present that the temporal decay of Tb^{3+} become fast with increasing the activators concentration. In the case of energy transfer, the luminescence lifetime of a sensitizer is shortened, because there are additional decay channels that shorten the lifetime of the excited state. Therefore, the decay lifetime of Tb^{3+} ions can be found to decrease with increase activators ions content, which is strong evidence for the energy transfer from the Tb^{3+} to activators.

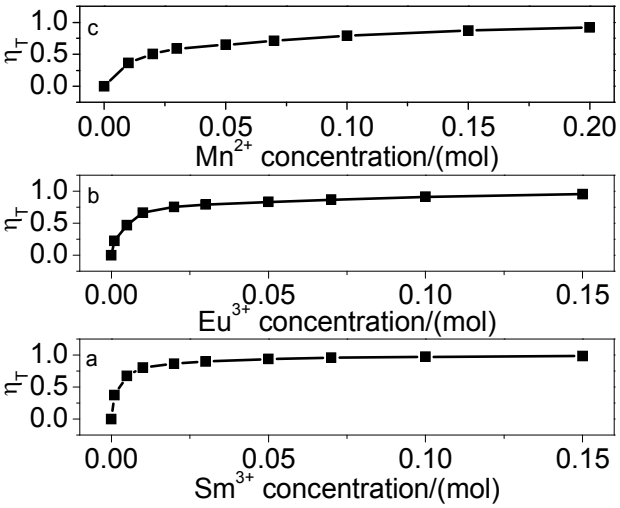

Figure 8. Energy transfer efficiencies (η_T) from Tb^{3+} to activators on concentrations in $Ba_3Tb_{1-x}(PO_4)_3$:xSm^{3+} (a), $Ba_3Tb_{1-y}(PO_4)_3$:yEu^{3+} (b) and $Ba_{3-z}Tb(PO_4)_3$:zMn^{2+} (c) (λ_{ex}=377 nm).

3.3 Energy transfer mechanism

In order to determine the energy transfer mechanisms from Tb^{3+} to activators in $Ba_3Tb(PO_4)_3$:Sm^{3+}, $Ba_3Tb(PO_4)_3$:Eu^{3+} and $Ba_3Tb(PO_4)_3$:Mn^{2+} samples, it is necessary to know the critical distance (R_c) between activators such as Sm^{3+}, Eu^{3+} and Mn^{2+}. With the increasing Sm^{3+}, Eu^{3+} and Mn^{2+} contents, the energy transfer from Tb^{3+} to activators becomes more efficient, and the probability of energy migration between activators increases simultaneously. When the distance is small enough, the concentration quenching occurs and the energy migration is hindered. The R_c value can be roughly assessed by the calculation pointed out by Blasse[36]

$R_c=2[3V/(4\pi X_cN)]^{1/3}$ (6)

where V corresponds to the volume of the unit cell, N is the number of host cations in the unit cell, and X_c is the critical concentration of dopant ions. For the $Ba_3Tb(PO_4)_3$, N=4, V=1140.6 Å and X_c is 0.02, 0.15, 0.03 for Sm^{3+}, Eu^{3+} (In our experiment, there is no concentration quenching of Eu^{3+} in $Ba_3Tb(PO_4)_3$, therefore, we select the maximum value) and Mn^{2+} respectively; Accordingly, the R_c are estimated to be about 30.08, 15.37, and 26.28 Å. In general, there are three mechanisms for noradiate energy transfer including exchange interaction, radiation reabsorption and electric multipolar interactions. The R_c obtained above indicate the little possibility of exchange interaction since the exchange interaction is predominant only for about 5 Å.[37] The mechanism of radiation reabsorption is only efficacious when the fluorescence and absorption spectra are widely overlapping, which also does not intend to occur in these cases. As a result, we can infer that the electric multipolar interactions would be responsible for the energy transfer mechanisms from the Tb^{3+} to activators. On account of Dexter's energy transfer formula of multipolar interactions and Reisfeld's approximation, the following relationship can be attained[38-41]

$(\eta_{S0}/\eta)\propto C^{\alpha/3}$ (7)

where η_0 and η are luminescence quantum efficiency of Tb^{3+} in the absence and presence of activators (Sm^{3+}, Eu^{3+} and Mn^{2+}), respectively; C is the concentration of Sm^{3+}, Eu^{3+} or Mn^{2+}. The value for α=6, 8, 10 corresponds to dipole-dipole, dipole-quadrupole, and quadrupole-quadrupole interactions, respectively. However, the

value of η_{S0}/η is hard to obtain, and thus it can be approximately estimated from the correlated intensity ratio (I_{S0}/I_S), where I_{S0} and I_S stand for the luminescence intensity of Tb^{3+} without and with the Sm^{3+}, Eu^{3+} and Mn^{2+} ions, respectively, the following relation can be achieved[38-41]

$$(I_{S0}/I) \propto C^{\alpha/3} \quad (8)$$

For $Ba_3Tb(PO_4)_3$:Sm^{3+}, $Ba_3Tb(PO_4)_3$:Eu^{3+} and $Ba_3Tb(PO_4)_3$:Mn^{2+}, the relationship between I_{S0}/I and $C^{\alpha/3}$ based on the above equation is illustrated in Figure 9a-j, which can be respectively fitted using straight line. One can find that all the biggest R^2 values of the linear fittings occur when α=6 in Figure 9a-j, corresponding to the best linear behaviours (a, d, h). Therefore, the energy transfers from the Tb^{3+} to Sm^{3+}, Eu^{3+} and Mn^{2+} ions take place through the dipole-dipole mechanisms.

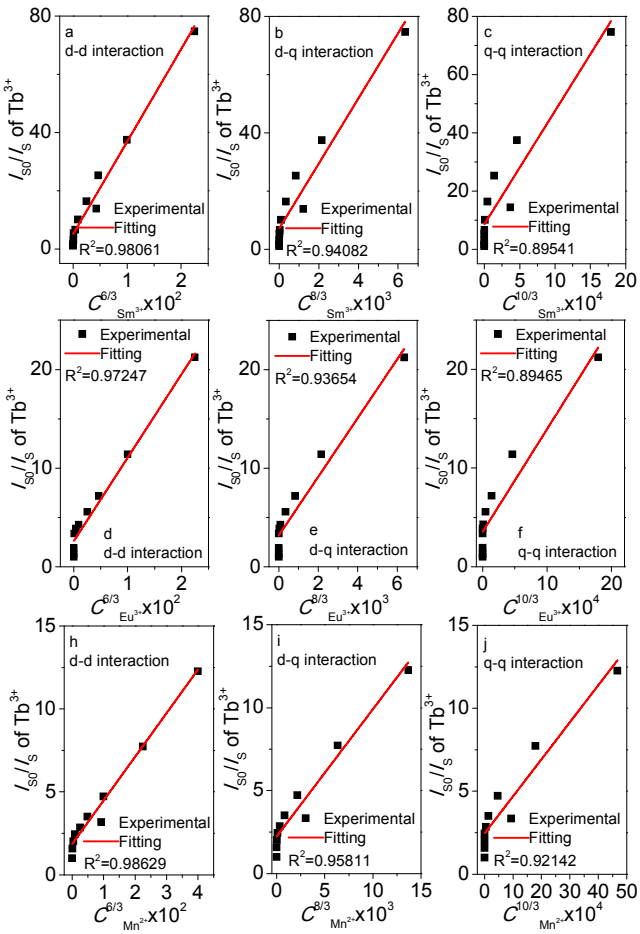

Figure 9. Dependence of I_{S0}/I_S of Tb^{3+} (a, d, h) $C^{6/3}$, (b, e, i) $C^{8/3}$, and (c, f, j) $C^{10/3}$.

Figure 10 shows a simple model expressing the energy transfer from Tb^{3+} to Sm^{3+}, Eu^{3+} and Mn^{2+} ions and the characteristic emission energy levels of Sm^{3+}, Eu^{3+} and Mn^{2+} in $Ba_3Tb(PO_4)_3$. In Sm^{3+}, Eu^{3+} and Mn^{2+} doped $Ba_3Tb(PO_4)_3$ samples, upon 377 nm radiation, $Ba_3Tb(PO_4)_3$ absorb UV radiation and then it transfer the energy to Sm^{3+}, Eu^{3+} and Mn^{2+} ions, which results in the increases of characteristic emission intensities of activators.

Table 1 depicts the corresponding CIE (Commission Intemationale de l'Eclairage 1931 chromaticity) coordinates positions and quantum efficiencies for the as-prepared $Ba_3Tb_{1-x}(PO_4)_3$:xSm^{3+} (x=0-0.15), $Ba_3Tb_{1-y}(PO_4)_3$:yEu^{3+} (y=0-0.15) and $Ba_{3-z}Tb(PO_4)_3$:zMn^{2+} (z=0-0.20) samples under 365 nm UV excitation (the emission color of phosphors can be seen from Figure 4-6). It can be found that the $Ba_3Tb_{1-x}(PO_4)_3$:xSm^{3+} can emit green to orange-red light, and their chromaticity coordinate varies from (0.3794, 0.5652) (x=0.001) to (0.5586, 0.4420) (x=0.15). The $Ba_3Tb_{1-y}(PO_4)_3$:yEu^{3+} can emit green to bright red, whose chromaticity coordinate changes from (0.3897, 0.5544) (y=0.001) to (0.6455, 0.3528) (y=0.15). The $Ba_{3-z}Tb(PO_4)_3$:zMn^{2+} (z=0-0.20) show the luminescence color varies from green to orange-red, for example, the chromaticity coordinate is from (0.3898, 0.5598) (z=0.001) to (0.5502, 0.4204) (z=0.20). Moreover, in all phosphors, the maximum quantum efficiency is 70.3% for $Ba_3Tb_{0.85}(PO_4)_3$:$0.15Eu^{3+}$.

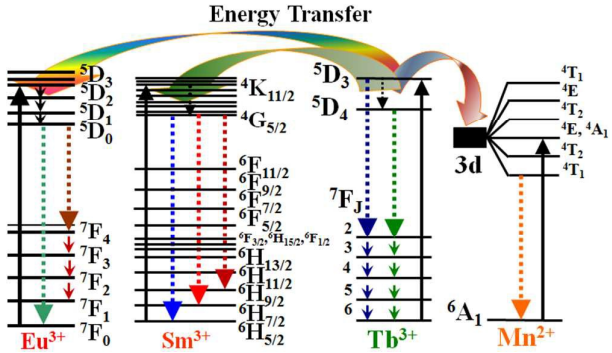

Figure 10. A simple model expressing the energy transfer from Tb^{3+} to activators (Sm^{3+}, Eu^{3+}, Mn^{2+}).

3.4 CIE Chromaticity Coordinate and Quantum efficiency

Table 1 Variation of Quantum Efficiency (QE) and CIE Chromaticity Coordinate of samples (λ_{ex}=377 nm)

Samples	CIE (X, Y)	CCT (K)	QE (%)
$Ba_3Tb(PO_4)_3$	(0.3196, 0.6009)	5889	51.2
$Ba_3Eu(PO_4)_3$	(0.6469, 0.3511)	1048	59.2
x=0.001	(0.3794, 0.5652)	4759	20.7
x=0.005	(0.3993, 0.5519)	4420	27.6
x=0.01	(0.4695, 0.4977)	3163	36.9
x=0.02	(0.4951, 0.4780)	2727	41.6
x=0.03	(0.5225, 0.4557)	2301	37.1
x=0.05	(0.5352, 0.4452)	2124	33.8
x=0.07	(0.5380, 0.4406)	2073	30.6
x=0.10	(0.5489, 0.4324)	1940	27.3
x=0.15	(0.5586, 0.4220)	1813	22.6
y=0.001	(0.3897, 0.5544)	4398	35.7
y=0.005	(0.4313, 0.5242)	3837	40.3
y=0.01	(0.4794, 0.4832)	2948	44.3
y=0.02	(0.5079, 0.4582)	2460	47.9

y=0.03	(0.5545, 0.4210)	1835	48.6
y=0.05	(0.5692, 0.4073)	1665	52.1
y=0.07	(0.6025, 0.3900)	1401	57.9
y=0.10	(0.6255, 0.3706)	1212	65.6
y=0.15	(0.6455, 0.3528)	1060	70.3
z=0.001	(0.3898, 0.5598)	4519	19.6
z=0.005	(0.4106, 0.5462)	3912	23.8
z=0.01	(0.4497, 0.5062)	3481	29.5
z=0.02	(0.4877, 0.4792)	2821	41.3
z=0.03	(0.5410, 0.4445)	2072	49.8
z=0.05	(0.5519, 0.4364)	1941	45.6
z=0.07	(0.5705, 0.4213)	1731	40.1
z=0.10	(0.5839, 0.4139)	1613	32.3
z=0.15	(0.5696, 0.4268)	1767	27.9
z=0.20	(0.5502, 0.4204)	1862	25.3

4 Conclusions

In summary, a series of Eu^{3+}, Sm^{3+} and Mn^{2+} ion doped $Ba_3Tb(PO_4)_3$ phosphors were synthesized via the conventional high temperature solid state method. $Ba_3Tb(PO_4)_3$ presents a cubic unit cell with space group I-43d. Under $^7F_6$-$^5D_3$ of Tb^{3+} excitation 377 nm, the emission intensities of $Ba_3Tb(PO_4)_3$:Sm^{3+}, $Ba_3Tb(PO_4)_3$:Eu^{3+} and $Ba_3Tb(PO_4)_3$:zMn^{2+} can be adjusted by changing the activators concentrations, and their emission color can also tuned from green to red or orange-red, which are attributed to the efficient energy transfer from Tb^{3+} to Sm^{3+}, Eu^{3+} and Mn^{2+}, respectively. The energy transfer mechanism was demonstrated to be the electric dipole-dipole interaction, and the best quantum efficiencies are 41.6%, 70.3% and 49.8% for $Ba_3Tb(PO_4)_3$:Sm^{3+}, $Ba_3Tb(PO_4)_3$:Eu^{3+} and $Ba_3Tb(PO_4)_3$:Mn^{2+} respectively. The results indicate that the phosphor may serve as potential red or orange-red emitting material for n-UV based white LEDs.

Acknowledgements

The work is supported by the National Natural Science Foundation of China (No.50902042), the Funds for Distinguished Young Scientists of Hebei Province, China (No.A2015201129), the Natural Science Foundation of Hebei Province, China (Nos.A2014201035, E2014201037), the Education Office Research Foundation of Hebei Province, China (Nos.ZD2014036, QN2014085), the Midwest Universities Comprehensive Strength Promotion Project.

Notes and references

1 Q. Zhou, Y. Zhou, Y. Liu, L. Luo, Z. Wang, J. Peng, J. Yan and M. Wu. J. Mater. Chem. C, 2015, 3, 3055-3059.
2 M. Peng, X. Yin, P. A. Tanner, M. G. Brik and P. Li. Chem. Mater., 2015, 27(8), 2938-2945.
3 Y. Wang, T. Wen, L. Tang, L. Yang, W. Yang and Y. Zhao. Dalton Trans., 2015, 44, 7578-7585.
4 J. Zhong, D. Chen, W. Zhao, Y. Zhou, H. Yu, L. Chen and Z. Ji . J. Mater. Chem. C, 2015, 3, 4500-4510.
5 H. Ji, Z. Huang, Z. Xia, M. S. Molokeev, X. Jiang, Z. Lin and V. V. Atuchin. Dalton Trans., 2015, 44, 7679-7686.
6 F. Baur, F. Glocker and T. Jüstel. J. Mater. Chem. C, 2015, 3, 2054-2064.
7 F. Kang, Y. Zhang, and M. Peng. Inorg. Chem., 2015, 54 (4), 1462-1473.
8 J. Zhang, Y. Liu, L. Li, N. Zhang, L. Zou and S. Gan. RSC Adv., 2015, 5, 29346-29352.
9 D. Wen, J. Feng, J. Li, J. Shi, M. Wu and Q. Su. J. Mater. Chem. C, 2015, 3, 2107-2114.
10 X. Min, Z. Huang, M. Fang, Y.-G. Liu, C. Tao and X. Wu. Inorg. Chem., 2014, 53, 6060-6065.
11 K. Li, X. Liu, Y. Zhang, X. Li, H. Lian and J. Lin. Inorg. Chem., 2015, 54 (1), 323-333.
12 D. Kang, H. S. Yoo, S. H. Jung, H. Kim and D. Y. Jeon. J. Phys. Chem. C, 2011, 115, 24334-24340.
13 Y.-C. Fang, S.-Y. Chu, P.-C. Kao, Y.-M. Chuang and Z.-L. Zeng. J. Electrochem. Soc., 2011, 158, J1-J5.
14 N. S. Singh, R. S. Ningthoujam, G. Phaomei, S. D. Singh, A. Vinu and R. K. Vatsa. Dalton Trans., 2012, 41, 4404-4412.
15 M. Shang, C. Li and J. Lin. Chem. Soc. Rev. 2014, 43, 1372-1386.
16 W. Lü, W. Lv, Q. Zhao, M. Jiao, B. Shao and H. You. J. Mater. Chem. C, 2015, 3, 2334-2340.
17 W. B. Dai. RSC Adv., 2014, 4, 11206-11215.
18 C. Zhang, H. Liang, S. Zhang, C. Liu, D. Hou, L. Zhou, G. Zhang, J. Shi. J. Phys. Chem. C, 2012, 116, 15932-15937.
19 N. Guo, Y. Jia, W. Lü, W. Lv, Q. Zhao, M. Jiao, B. Shao and H. You. Dalton Trans., 2013, 42, 5649-5654.
20 N. Guo, Y. Huang, Y. Jia, W. Lv, Q. Zhao, W. Lü, Z. Xia and H. You. Dalton Trans., 2013, 42 , 941-947.
21 V. B. Mikhailik and H. Kraus. J. Lumin., 2009, 129, 945-947.
22 Y. Jia, W. Lü, N. Guo, W. Lü, Q. Zhao and H. You. Phys. Chem. Chem. Phys., 2013, 15, 6057-6062.
23 Z. Wang, S. Lou and P. Li. J. Lumin., 2014, 156, 87-90.
24 T. W. Kuo and T. M. Chen. J. Electrochem. Soc., 2010, 157, J216-J220.
25 M. Jiao, N. Guo, W. Lü, Y. Jia, W. Lv, Q. Zhao, B. Shao and H. You. Dalton Trans., 2013, 42, 12395-12402.
26 X. Chen, Z. Gong, Q. Wan, S. Wu, F. Guo, N. Zhuang and J. Chen. Opt. Mater., 2015, 44, 48-53.
27 Z. Xia, Y. Zhang, M. S. Molokeev and V. V. Atuchin. J. Phys. Chem. C, 2013, 117, 20847-20854.
28 H. Lin, E. Y. B. Pun, L. H. Huang and X. R. Liu. Appl. Phys. Lett., 2002, 80, 2642-2644.
29 W.-J. Yang and T.-M. Chen. Appl. Phys. Lett., 2006, 88, 101903.
30 K. H. Kwon, W. B. Im, H. S. Jang, H. S. Yoo and D. Y. Jeon. Inorg. Chem., 2009, 48, 11525-11532.
31 P. I. Paulose, G. Jose, V. Thomas, N. V. Unnikrishnan and M. K. R. Warrier. J. Phys. Chem. Solids, 2003, 64, 841-846.
32 W. J. Yang, L. Luo, T. M. Chen and N. S. Wang. Chem. Mater., 2005, 17, 3883-3888.
33 C.-H. Huang, T.-M. Chen, W.-R. Liu, Y.-C. Chiu, Y.-T. Yeh and S.-M. Jang. ACS Appl. Mater. Interfaces, 2010, 2, 259-264.
34 C.-H. Huang and T.-M. Chen. J. Phys. Chem. C, 2011, 115, 2349-2355.
35 C. H. Huang and T.-M. Chen. Opt. Express, 2010, 18, 5089-5099.
36 G. Blasse. Phys. Lett. 1968, 28A, 444-445.
37 G. Blasse and B. C. Grabmaier. Luminescent Materials, Berlin: Springer, 1994.
38 D. L. Dexter and J. H. Schulman. J. Chem. Phys., 1954, 22, 1063-1070.
39 R. Reisfeld, E. Greenberg, R. Velapoldi and B. Barnett. J. Chem. Phys., 1972, 56, 1698-1705.
40 U. Caldiño, J. L. Hernández-Pozos, C. Flores, A. Speghini and M. Bettinelli. J. Phys.: Condens. Matter, 2005, 17, 7297-7306.
41 J. Zhang, Y. He, Z. Qiu, W. Zhang, W. Zhou, L. Yu and S. Lian. Dalton Trans., 2014, 43, 18134-18145.